Topological thermal Hall effect and nondissipative transport of the nanometric skyrmion lattice in Gd2PdSi3

Daiki Yamaguchi, Parisa Mokhtari, Rinsuke Yamada, Akiko Kikkawa, Yasujiro Taguchi, Yoshinori Tokura, Max Hirschberger

Angaben zur Veröffentlichung / Publication details:

Yamaguchi, Daiki, Parisa Mokhtari, Rinsuke Yamada, Akiko Kikkawa, Yasujiro Taguchi, Yoshinori Tokura, and Max Hirschberger. 2026. "Topological thermal Hall effect and nondissipative transport of the nanometric skyrmion lattice in Gd2PdSi3." *PNAS Nexus* 5 (3): pgag041. https://doi.org/10.1093/pnasnexus/pgag041.

PNAS NEXUS

PNAS Nexus, 2026, **5**, pgag041

https://doi.org/10.1093/pnasnexus/pgag041
Advance access publication 23 February 2026
Research Report

Topological thermal Hall effect and nondissipative transport of the nanometric skyrmion lattice in Gd_2PdSi_3

Daiki Yamaguchi [a,*,1], Parisa Mokhtari [a,b,1], Rinsuke Yamada [a], Akiko Kikkawa [c], Yasujiro Taguchi [c], Yoshinori Tokura [a,c,d] and Max Hirschberger [a,c,*]

[a]Department of Applied Physics and Quantum-Phase Electronics Center (QPEC), The University of Tokyo, 7-3-1 Hongo, Bunkyo-ku, Tokyo 113-8656, Japan
[b]Center for Electronic Correlations and Magnetism, Institute of Physics, University of Augsburg, 86159 Augsburg, Germany
[c]RIKEN Center for Emergent Matter Science (CEMS), 2-1 Hirosawa, Wako, Saitama 351-0198, Japan
[d]Tokyo College, The University of Tokyo, 7-3-1 Hongo, Bunkyo-ku, Tokyo 113-8656, Japan
*To whom correspondence should be addressed: Email: dai20yama011-1@g.ecc.u-tokyo.ac.jp (D.Y.); Email: hirschberger@ap.t.u-tokyo.ac.jp (M.H.)
[1]D.Y. and P.M. contributed equally to this work.
Edited By Jainendra Jain

Abstract

We report the first observation of a topological thermal Hall effect (tTHE) of electrons moving through a magnetic skyrmion lattice (SkL) of short period, where the skyrmion diameter is only a few nanometers. In the hexagonal intermetallic Gd_2PdSi_3, we observe a characteristic anomaly in the magnetic field dependence of the thermal Hall conductivity κ_{xy}, which scales well with the anomaly in the electrical Hall conductivity σ_{xy} and is closely related to the topological winding number of the SkL ground state. The relative magnitude of entropy and charge currents, defined as the Lorenz ratio $\sim \kappa_{xy}/(\sigma_{xy}T)$, is consistent with a nondissipative, or intrinsic, mechanism for the topological Hall effect. We stress that the Berry phase in momentum space ($\boldsymbol{k}$-space) causes such a nondissipative Hall transport, independent of the carrier relaxation time.

Keywords: thermal Hall effect, nanometric skyrmion, nondissipative topological transport, Lorenz ratio

Significance Statement

The transverse thermal gradient induced by longitudinal heat current, thermal Hall effect, is precisely measured in a material with a spin vortex lattice of nanometric modulation period. The Hall effect is called topological, as it is related to the quantum geometric curvature of spin texture, and is anticipated to be free of energy loss. In this report, the scaling between thermal and electrical Hall conductivities confirms the energy-loss-less nature of the topological Hall electronic current. This provides an experimental clarification of the nondissipative nature of the topological quantum current for future energy efficient electronics.

Introduction

A key trend in contemporary research on solids is the detection of a fictitious Lorentz force, or emergent magnetic field, through the measurement of heat carried by fundamental excitations. The transverse deflection of heat current density $\boldsymbol{J}^{Q}$ due to this Lorentz force is picked up in experiments as a thermal Hall effect $J_y^Q = \kappa_{xy}(\partial_x T)$, where $(-\partial_x T)$ is the temperature gradient applied along a sample. For lattice vibrations (phonons), thermal Hall conductivity κ_{xy} can be caused by extrinsic skew scattering from magnetic or charged defects (1, 2), or by intrinsic quantum phenomena related to the coupling of spin waves (magnons) and phonons (3, 4). Both sources of phononic κ_{xy} explored so far can be traced back to relativistic spin-orbit coupling (SOC). Spin waves in long-range ordered magnets create κ_{xy} due to SOC or due to the non-coplanar twisting of magnetic spins in space, termed scalar spin chirality (5). If the magnetic unit cell is large enough, and if the magnetization can be considered as a continuous field $\boldsymbol{n}$ in space, which is normalized to unit length, there is a contribution to κ_{xy} directly proportional to the topological charge

$$n_{sk} = \frac{1}{4\pi}\int \boldsymbol{n}\cdot\left(\frac{\partial \boldsymbol{n}}{\partial x}\times\frac{\partial \boldsymbol{n}}{\partial y}\right)\mathrm{d}x\mathrm{d}y. \quad (1)$$

For example, magnonic $\kappa_{xy} \propto n_{sk}$ has been observed in skyrmion-hosting insulators recently (6, 7).

In this work, we focus on the κ_{xy} of *electrons* due to n_{sk}. Figure 1A illustrates the anomalous κ_{xy} in metallic ferromagnets, which is attributed to SOC and has been thoroughly studied (8–10). However, the observation of an electronic κ_{xy} for a magnetic skyrmion lattice (SkL), where κ_{xy} is directly related to n_{sk} as illustrated in Fig. 1B, has remained an open challenge in the field. We report

Competing Interest: The authors declare no competing interests.
Received: August 7, 2025. **Accepted:** January 24, 2026

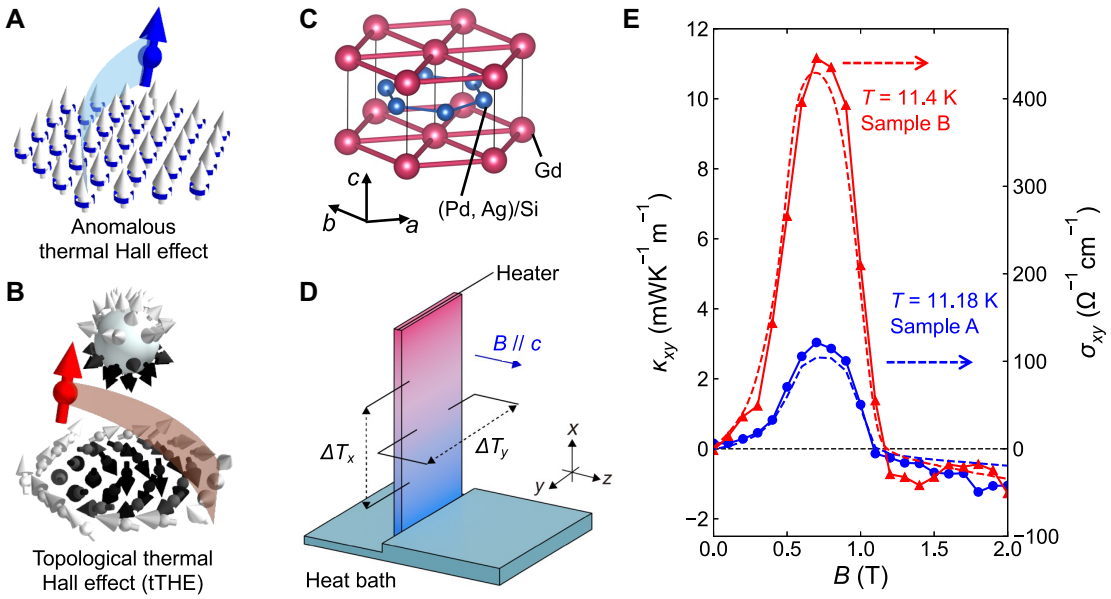

Fig. 1. Topological thermal Hall effect (tTHE) of skyrmions in Gd_2PdSi_3. A, B) Anomalous thermal Hall effect and tTHE (schematic) have opposite signs in Gd_2PdSi_3; the former is too small to be easily visible in the data. The itinerant conduction electron is represented in blue/red large sphere with fat arrow, and the blue circles around individual atoms in (A) represent the orbital angular momentum that is essential for the former effect. C) Schematic crystal structure of Gd_2PdSi_3. D) Setup for thermal Hall effect measurement. The plate-shape sample (red/blue plate) connects heater (top) and heat bath (light blue plate); thermometers detect longitudinal (ΔT_x) and transverse (ΔT_y) temperature gradients. The magnetic field (B) is applied perpendicular to the sample plane (along the c-axis). E) Magnetic field dependence of thermal (κ_{xy}, symbols) and electrical (σ_{xy}, dashed lines) Hall effects in pristine and lightly electron-doped Gd_2PdSi_3 (samples A and B, respectively). The σ_{xy} scale (right) is stretched to match the κ_{xy}.

the topological thermal Hall effect (tTHE) of electrons under the influence of n_{sk} in the SkL of Gd_2PdSi_3. Our analysis of energy dissipation based on the Lorenz ratio of entropy and charge conductivities confirms that κ_{xy} is not affected by inelastic scattering, consistent with an intrinsic and nondissipative mechanism for the topological Hall effect in Gd_2PdSi_3 (11). We discuss the general relevance of this electronic tTHE as a testing bed for adiabatic spin transport and the theory of spin-Berry phases in solids.

Results

Topological thermal Hall effect and Lorenz ratio

Figure 1C shows the hexagonal AlB_2-type structure of Gd_2PdSi_3 (12, 13). The crystal is built of magnetic layers comprising a triangular lattice of Gd^{3+} atoms, sandwiched by nonmagnetic honeycomb layers of Pd/Si. The highly symmetric crystal structure and weak magnetic anisotropy of Gd^{3+} ions allow the formation of a SkL with nanometric magnetic vortices of 2–3 nm arrayed in the hexagonal basal plane (ab-plane) of Gd_2PdSi_3. Here, electronic states have significant Gd-5d character, resulting in a strong exchange coupling between local magnetic moments and the spin of conducting states on the order of several 100 meV (14–16).

Figure 1D illustrates the setup for the thermal Hall effect measurement. A heat current $\boldsymbol{J}^{Q}$ is applied to the plate-shape sample along the negative x-direction. The magnetic field $\boldsymbol{B}$ is perpendicular to the sample plane (along the z-direction). Note that the z-direction in Fig. 1D corresponds to the c-axis of the hexagonal structure (Fig. 1C). See also Materials and methods section and Supplementary material for more detail.

Figure 1E shows representative results of tTHE (κ_{xy}) and electrical Hall effect (σ_{xy}) around 11 K for two single crystals of Gd_2PdSi_3: sample A (pristine) and sample B (5% Ag substitution for Pd, slightly electron-doped). Here, the electrical conductivity tensor is defined as $J_i = \sigma_{ij}E_j$, where $\boldsymbol{J}$ and $\boldsymbol{E}$ are the electric current density and the electric field, respectively. The general shape of σ_{xy} and κ_{xy} is closely comparable, with a flat-top profile suggestive of the calculated behavior of $n_{sk}(B)$ for a SkL state induced by magnetic field (17, 18). We also note that κ_{xy} and σ_{xy} have the same sign throughout the experimentally accessible range of temperature and magnetic field.

To set the stage for a more quantitative analysis of these results, we discuss the temperature dependence of σ_{xx} and κ_{xx} in Fig. 2A. Analyzing the thermal transport data from the viewpoint of the generalized Lorenz ratio,

$$\mathcal{L}_{ij} = \frac{\kappa_{ij}}{\sigma_{ij}T}, \tag{2}$$

we start by focusing on $\mathcal{L}_{xx}$. Note that the thermal conductivity is considered to have phonon and electron contributions: $\kappa_{xx} = \kappa_{xx}^{ph} + \kappa_{xx}^{el}$. When $\kappa_{xx}^{el} \gg \kappa_{xx}^{ph}$, $\mathcal{L}_{xx}$ is expected to approach the Lorenz number $\mathcal{L}_0 = (\pi^2/3)(k_B/e)^2$ at low T (19); we observe $\mathcal{L}_{xx} > 15 \times \mathcal{L}_0$ in the accessible temperature range (Fig. 2B) and infer that κ_{xx}^{ph} cannot be ignored in the heat transport of Gd_2PdSi_3. Moreover, magnon heat flow seems to be negligible, as there is no clear anomaly or enhancement in $\kappa_{xx}(T)$ below $T_N \sim 20$ K (see also Fig. S6A).

Further attempting to isolate the electronic term, we move on to $\mathcal{L}_{xy}$. In conductors, the electrons' contribution to the thermal Hall conductivity is expected to dominate: $\kappa_{xy} \approx \kappa_{xy}^{el}$, and $\mathcal{L}_{xy}$ should also approach $\mathcal{L}_0$ as $T \to 0$ (20). Figure 2C–J overplots κ_{xy}/T and $\sigma_{xy}\,\mathcal{L}_0$, which are the constituent parts of $\mathcal{L}_{xy}/\mathcal{L}_0$. Over the entire temperature range, the curves track each other well for both A and B, especially in the low magnetic field region of the SkL state. In contrast, there is a significant temperature-

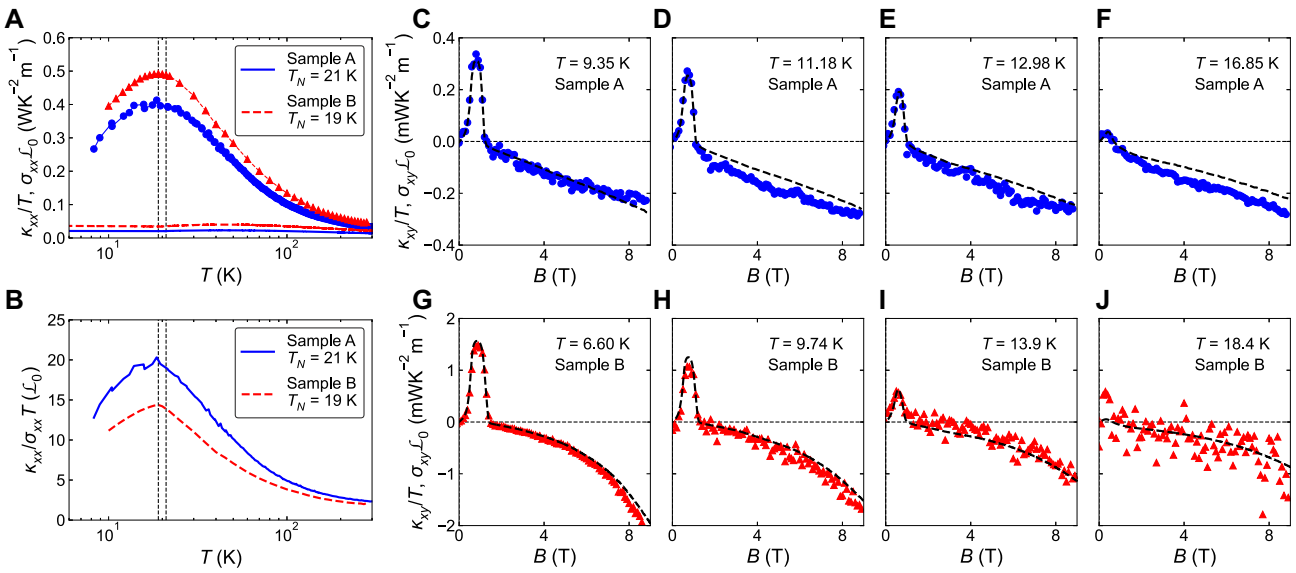

Fig. 2. Temperature and magnetic field dependence of tTHE. A) Temperature (T) dependence of κ_{xx}/T, $\sigma_{xx}\mathcal{L}_0$, where $\mathcal{L}_0 = (\pi^2/3)(k_B/e)^2$ is the Lorenz number. Blue circles (solid lines) and red triangles (dashed lines) indicate κ_{xx}/T ($\sigma_{xx}/\mathcal{L}_0$) of samples A and B of Gd_2PdSi_3, respectively. B) T dependence of $\kappa_{xx}/\sigma_{xx}T$ in units of $\mathcal{L}_0$. Blue solid and red dashed lines correspond to samples A and B, respectively. The vertical black dashed lines in (A) and (B) indicate the transition temperature T_N of each sample. C–J) Magnetic field dependence of κ_{xy}/T (blue circles and red triangles) and $\sigma_{xy}\mathcal{L}_0$ (fat black dashed lines) in sample A (C–F) and sample B (G–J) of Gd_2PdSi_3 at various $T < T_N$.

dependent separation between κ_{xy}/T and $\sigma_{xy}\mathcal{L}_0$ in the high magnetic field region. Encouragingly, these results suggest that a discussion using $\mathcal{L}_{xy}$ may be applicable for the tTHE in Gd_2PdSi_3, indicating that the topological Hall transport in the SkL state is distinct from the normal Hall transport, as discussed in the following.

Nondissipative transport

We separate the thermal Hall conductivity into two contributions: (i) the normal Hall channel, from orbital motion in the applied external field B and (ii) the topological Hall channel, arising from the topological winding number n_{sk} of the SkL; *viz.* $\kappa_{xy} = \kappa_{xy}^{N} + \kappa_{xy}^{T}$. The κ_{xy}^{T} is responsible for the enhancement of κ_{xy} within the SkL state, while κ_{xy}^{N} dominates at high-B. Likewise, σ_{xy} is written as a sum of two terms, since the anomalous Hall effect from the net magnetization and SOC is very weak in Gd_2PdSi_3 (18). Accordingly, for each sample, Fig. 3A and B shows the T dependence of κ_{xy}/T and $\sigma_{xy}\mathcal{L}_0$ at their peak value in the SkL phase, representing the topological component. Moreover, the figure also shows κ_{xy}/T and $\sigma_{xy}\mathcal{L}_0$ at $B = 8$ T, corresponding to the normal (thermal) Hall effect. Thus, the high field and peak values are identified with κ_{xy}^{N} (σ_{xy}^{N}) and κ_{xy}^{T} (σ_{xy}^{T}), respectively. We further define a Lorenz ratio $\mathcal{L}^{T}$ for the tTHE by setting $\sigma_{ij} = \sigma_{xy}^{T}$ and $\kappa_{ij} = \kappa_{xy}^{T}$ in Eq. 2 and plot it as a function of T in Fig. 3C: $\mathcal{L}^{T}$ is found to be close to $\mathcal{L}_0$ at low temperatures. From now on, we focus on $\mathcal{L}^{T}$ in the SkL state; the Lorenz ratio for the normal Hall effect, $\mathcal{L}^{N}$, is analyzed in the Supplementary material, where a stronger temperature dependence is observed, with a deviation from $\mathcal{L}_0$.

What is the physical importance of $\mathcal{L}_{xy}^{T} \sim \mathcal{L}_0$? The insets in Fig. 3C show schematic illustrations of charge and entropy flow in momentum ($\boldsymbol{k}$-) space. In principle, electrons carry both charge $-e$ and entropy $k_B T$ at the same rate as they move in a crystal. The derivation of $\mathcal{L}_{ij} = \mathcal{L}_0$ at low T rests on the assumption that there is a fixed relation between loss of momentum and kinetic energy in the relevant scattering processes that relax the (charge or heat) current (19). This is generally true for elastic scattering but certain inelastic scattering processes—from above to below the Fermi energy E_F—dramatically change the kinetic energy of a moving electron, while they hardly change its momentum. Assuming that electrons dominate both heat and charge currents, inelastic scattering causes $\mathcal{L}_{ij} < \mathcal{L}_0$.

Hall effect from Berry phase in momentum space

Quantum mechanical wave propagation of elementary excitations in solids can create nondissipative charge or entropy currents, as modeled by the Berry phase. These currents are by definition insensitive to inelastic scattering processes (energy loss). In the nondissipative case, $\mathcal{L}_{xy}^{T}/\mathcal{L}_0 = 1$ is realized even when electrons are involved in inelastic scattering from phonons, spin waves, or other excitations in solids. Under the influence of relativistic SOC, the σ_{xy} and κ_{xy} in electron transport of ferromagnets (24), and of noncollinear antiferromagnets (25, 26) have been shown to be independent of the carrier relaxation time τ, including inelastic scattering. The topological charge n_{sk} provides one route to realize σ_{xy} and κ_{xy} without the need for SOC (23). In the limit where the magnetic skyrmions are much larger than a crystallographic unit cell, electrons move under the influence of a Berry phase in real space ($\boldsymbol{r}$-space approximation) (27–30). Here, $\sigma_{xy}^{T} \propto n_{sk}$ depends on τ and a deviation from $\mathcal{L}_{xy}^{T}/\mathcal{L}_0 = 1$ is expected (23, 27, 29). Figure 1B in fact illustrates electron flow in this approximation, where wavepackets of Bloch electrons move through a twisted magnetic background, adiabatically adjusting their spin to the local quantization axis. When the skyrmion is small enough, Berry phases should be considered in $\boldsymbol{k}$-space and σ_{xy} is predicted to be independent of τ; this is the limit of clean crystals, where the mean-free path is comparable to or larger than the size of a skyrmion (21, 31, 32). Our analysis of the Lorenz ratio shows $\mathcal{L}_{xy}^{T}/\mathcal{L}_0 \sim 1$, in both our samples of Gd_2PdSi_3, which indicates that there is no significant effect of inelastic scattering processes on κ_{xy}^{T}. Thus, the $\boldsymbol{k}$-space limit for

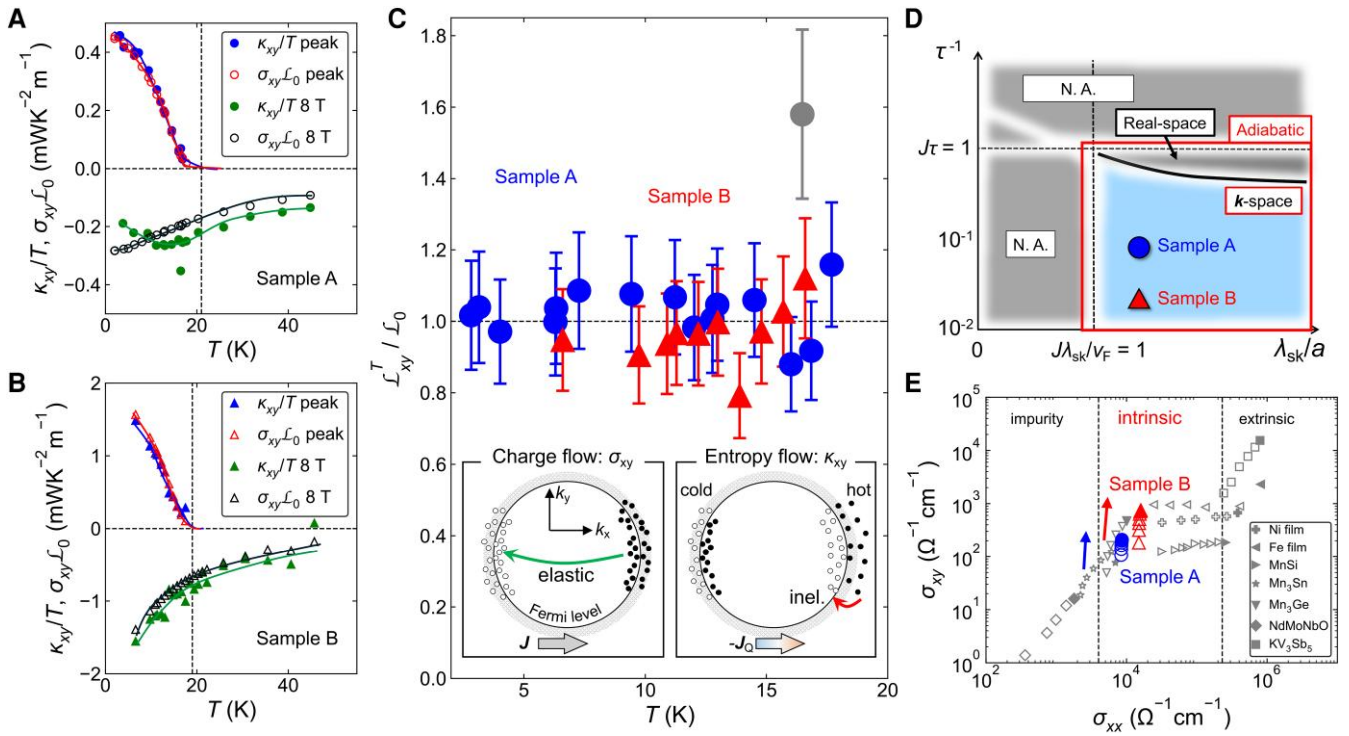

Fig. 3. Lorenz ratio for the tTHE in Gd_2PdSi_3. A, B) For samples A and B, we show the peak values of tTHE (κ_{xy}/T) and electrical topological Hall effect ($\sigma_{xy}\mathcal{L}_0$) in the SkL phase (positive, red and blue) and the high-field values at $B = 8$ T (negative, green and black). C) T-dependence of the topological Hall Lorenz ratio ($\mathcal{L}^{T}_{xy}/\mathcal{L}_0$) in sample A (blue circles) and sample B (red triangles). An outlier is shown in gray color. Inset of (C): elastic and inelastic electronic scattering processes for charge current $\boldsymbol{J}$ and entropy current $\boldsymbol{J}_Q$ (see text). Solid and open circles represent occupied (filled) and empty states (holes), respectively. D) Parameter space of Matsui et al. (21), where J, v_F, τ, λ_{sk}, and a are the coupling strength between itinerant and local moments, Fermi velocity, carrier relaxation time, and sizes of magnetic and crystallographic unit cells, respectively. Points are placed for sample A (blue circle) and sample B (red triangle). E) Logarithmic plot of electrical Hall conductivity σ_{xy} vs. electrical conductivity σ_{xx} for materials with a Hall effect of magnetic origin, following Refs. (22, 23). We add corresponding symbols for the topological Hall effect of Gd_2PdSi_3, where the change with T (red and blue arrows) relates to a T-dependent change of the ordered moment—not a change of σ_{xx}. The solid symbols mark the values at base-T for sample A and B, which are most relevant to the scaling analysis. Dashed lines: impurity scattering, intrinsic, and extrinsic regimes of the anomalous Hall effect.

the topological Hall current is appropriate in Gd_2PdSi_3, rather than the $\boldsymbol{r}$-space approximation.

Matsui et al. (21) discuss the crossover between $\boldsymbol{r}$-space approximation and the $\boldsymbol{k}$-space limit from the viewpoint of a simple one-band model. We adopt the essence of their analysis in Fig. 3D, where the right-hand side corresponds to the limit of large skyrmion size (λ_{sk}), while on the vertical axis, the upper side corresponds to the disordered limit with shorter mean-free-path. Here, clean materials with small skyrmions are classified into the $\boldsymbol{k}$-space regime with adiabatic coupling of conduction electron spin and local moment. Consistent with the analysis of the Lorenz ratio $\mathcal{L}^{T}_{xy}$, our samples A and B of Gd_2PdSi_3 are estimated to be in the $\boldsymbol{k}$-space regime based on $\lambda_{sk} = 2.5$ nm, Fermi velocity $v_F = 5.3 \times 10^5$ ms^{-1}, exchange coupling strength $J = 0.2$ eV, and relaxation time $\tau = 44$ fs (sample A) and 18 fs (sample B) from Refs. (16, 33).

Another perspective on the intrinsic or nondissipative $\boldsymbol{k}$-space regime is provided by the universal scaling law of σ_{xy} versus σ_{xx} for the Hall effect, as proposed by Onoda et al. (22, 23). Figure 3E emphasizes the moderately dirty, *intrinsic* regime: $3 \times 10^3 < \sigma_{xx} < 5 \times 10^5\ \Omega^{-1}\mathrm{cm}^{-1}$ in good metals. Here, the Hall current is directly related to the Berry phase of conduction electrons in $\boldsymbol{k}$-space, with only minor contamination by extrinsic effects, such as skew scattering. Samples A and B of Gd_2PdSi_3 are located at around $10^4\ \Omega^{-1}\,\mathrm{cm}^{-1}$, within the intrinsic regime. Note that the carrier density of $\approx 10^{22}\ \mathrm{cm}^{-3}$ in Gd_2PdSi_3 (16, 34) is comparable to typical metals, such as elemental Fe (35). This scaling plot is designed in relation to defect (quenched impurity) scattering, and thus σ_{xx} on the horizontal axis essentially relates to the relaxation time τ.

Discussion

In conclusion, we report the first example of an electronic tTHE in a SkL host. In Gd_2PdSi_3, the entropy and charge currents of electrons passing through the nanometric SkL are directly proportional to each other, establishing $\mathcal{L}^{T}_{xy} \sim \mathcal{L}_0$ for the tTHE. On the other hand, the Lorenz ratio for the normal Hall conductivity from conventional orbital motion of conduction electrons, $\mathcal{L}^{N}_{xy}$, shows stronger temperature dependence, possibly due to a contributions from the phonon thermal Hall effect (36, 37) and from inelastic magnetic scattering (38–40) (see Supplementary material for detailed discussion). This contrast between $\mathcal{L}^{T}_{xy}$ and $\mathcal{L}^{N}_{xy}$ further confirms that inelastic scattering processes do not contribute to the relaxation of the topological Hall current in Gd_2PdSi_3. Our finding supports the intrinsic ($\boldsymbol{k}$-space limit) scenario for the tTHE from electron transport through a nanometric SkL (11), rather than the $\boldsymbol{r}$-space approximation that was developed for large-scale spin superstructures in MnSi and related SkL hosts.

Materials and methods

Single crystals of Gd_2PdSi_3 are obtained by the high-vacuum optical floating zoning method (16). A plate-shape sample is cut

from the crystal and set up to connect between the heat bath and a metal film heater, subject to a heat current J^Q along the negative x-direction as in Fig. 1D. The longitudinal (ΔT_x) and transverse (ΔT_y) temperature differences are measured with semiconducting chip thermometers and converted to thermal conductivity κ_{xx} and thermal Hall conductivity κ_{xy} (see Supplementary material for more detail). For measurements of the electrical conductivity σ_{xx} and the Hall conductivity σ_{xy}, we use the same sample plate with the same contacts, wires, etc., as those for thermal conductivity measurements. We additionally calibrate the absolute values of κ_{xx} and σ_{xx} using zero-field measurements on bar-shape samples.

Acknowledgments

We acknowledge Y. Takahashi, Y. Okamura, and Y. Kato for providing us with their optical conductivity data for the relaxation time estimation of Gd_2PdSi_3. We thank T. Kurumaji for fruitful discussions.

Supplementary Material

Supplementary material is available at *PNAS Nexus* online.

Funding

P.M. and M.H. are supported by the Deutsche Forschungsgemeinschaft (DFG, German Research Foundation) via Transregio TRR 360 - 492547816. Y.Ta. is supported by the RIKEN TRIP initiative (Many-body Electron Systems and Advanced General Intelligence for Science Program). This work was supported by JSPS KAKENHI grant nos. JP22K20348, JP23H05431, JP23K13057, JP24H01607, JP24H01604, and JP25K17336. It was also supported by the Japan Science and Technology Agency via JST CREST grant nos. JPMJCR1874 and JPMJCR20T1 (Japan), JST FOREST grant no. JPMJFR2238 (Japan), and JST Adopting Sustainable Partnerships for Innovative Research Ecosystem (ASPIRE) grant no. JPMJAP2426. The authors are grateful for support from the Murata Science Foundation, the Yamada Science Foundation, the Hattori Hokokai Foundation, the Iketani Science and Technology Foundation, the Mazda Foundation, the Casio Science Promotion Foundation, the Takayanagi Foundation, and the Yashima Environment Technology Foundation.

Author Contributions

M.H. conceived and supervised the project. D.Y., P.M., and R.Y. performed thermal and electrical transport measurements, data analysis/visualization, and calculation. A.K. grew single crystals. D.Y., P.M., and M.H. wrote the original draft. Y.Ta. and Y.To. reviewed and edited the draft. All authors discussed the results and commented on the manuscript.

Data Availability

All data needed to evaluate the conclusions in the article are present in the article and/or Supplementary material.

References

1 Strohm C, Rikken GLJA, Wyder P. 2005. Phenomenological evidence for the phonon Hall effect. *Phys Rev Lett*. 95(15):155901.
2 Flebus B, MacDonald AH. 2022. Charged defects and phonon Hall effects in ionic crystals. *Phys Rev B*. 105(22):L220301.
3 Chen J-Y, Kivelson SA, Sun X-Q. 2020. Enhanced thermal Hall effect in nearly ferroelectric insulators. *Phys Rev Lett*. 124(16):167601.
4 Mangeolle L, Balents L, Savary L. 2022. Phonon thermal Hall conductivity from scattering with collective fluctuations. *Phys Rev X*. 12:041031.
5 Katsura H, Nagaosa N, Lee PA. 2010. Theory of the thermal Hall effect in quantum magnets. *Phys Rev Lett*. 104(6):066403.
6 Akazawa M, *et al.* 2022. Topological thermal Hall effect of magnons in magnetic skyrmion lattice. *Phys Rev Res*. 4(4):043085.
7 Takeda H, *et al.* 2024. Magnon thermal Hall effect via emergent SU(3) flux on the antiferromagnetic skyrmion lattice. *Nat Commun*. 15(1):566.
8 Shiomi Y, Onose Y, Tokura Y. 2010. Effect of scattering on intrinsic anomalous Hall effect investigated by Lorenz ratio. *Phys Rev B*. 81(5):054414.
9 Xu L, *et al.* 2020. Anomalous transverse response of Co_2MnGa and universality of the room-temperature $\alpha_{ij}^A/\sigma_{ij}^A$ ratio across topological magnets. *Phys Rev B*. 101(18):180404(R).
10 Ding L, *et al.* 2021. Quantum oscillations, magnetic breakdown and thermal Hall effect in $Co_3Sn_2S_2$. *J Phys D Appl Phys*. 54(45):454003.
11 Chen H-Y, Nomoto T, Hirschberger M, Arita R. 2025. Topological Hall effect of skyrmions from first principles. *Phys Rev X*. 15:011054.
12 Nentwich M, *et al.* 2020. Structure variations within RSi_2 and R_2TSi_3 silicides. Part I. structure overview. *Acta Crystallogr B*. 76(2):177–200.
13 Spitz L, *et al.* 2022. Entropy-assisted, long-period stacking of honeycomb layers in an AlB_2-type silicide. *J Am Chem Soc*. 144(37):16866–16871.
14 Bouaziz J, Mendive-Tapia E, Blügel S, Staunton JB. 2022. Fermi-surface origin of skyrmion lattices in centrosymmetric rare-earth intermetallics. *Phys Rev Lett*. 128(15):157206.
15 Nomoto T, Koretsune T, Arita R. 2020. Formation mechanism of the helical **Q** structure in Gd-based skyrmion materials. *Phys Rev Lett*. 125(11):117204.
16 Hirschberger M, *et al.* 2020. Topological nernst effect of the two-dimensional skyrmion lattice. *Phys Rev Lett*. 125(7):076602.
17 Okubo T, Chung S, Kawamura H. 2012. Multiple-*q* states and the skyrmion lattice of the triangular-lattice Heisenberg antiferromagnet under magnetic fields. *Phys Rev Lett*. 108(1):017206.
18 Kurumaji T, *et al.* 2019. Skyrmion lattice with a giant topological Hall effect in a frustrated triangular-lattice magnet. *Science*. 365(6456):914.
19 Ziman JM. *Principles of the theory of solids*. 2nd ed. Cambridge University Press, Cambridge, 1979.
20 Zhang Y, *et al.* 2000. Determining the Wiedemann-Franz ratio from the thermal Hall conductivity: application to Cu and $YBa_2Cu_3O_{6.95}$. *Phys Rev Lett*. 84(10):2219.
21 Matsui A, Nomoto T, Arita R. 2021. Skyrmion-size dependence of the topological Hall effect: a real-space calculation. *Phys Rev B*. 104(17):174432.
22 Onoda S, Sugimoto N, Nagaosa N. 2008. Quantum transport theory of anomalous electric, thermoelectric, and thermal Hall effects in ferromagnets. *Phys Rev B*. 77(16):165103.
23 Nagaosa N, Sinova J, Onoda S, MacDonald AH, Ong NP. 2010. Anomalous Hall effect. *Rev Mod Phys*. 82(2):1539.
24 Onose Y, Shiomi Y, Tokura Y. 2008. Lorenz number determination of the dissipationless nature of the anomalous Hall effect in itinerant ferromagnets. *Phys Rev Lett*. 100(1):016601.

25 Xu L, *et al.* 2020. Finite-temperature violation of the anomalous transverse Wiedemann-Franz law. *Sci Adv*. 6(17):eaaz3522.
26 Li X, *et al.* 2017. Anomalous Nernst and Righi-Leduc effects in Mn_3Sn: Berry curvature and entropy flow. *Phys Rev Lett*. 119(5): 056601.
27 Neubauer A, *et al.* 2009. Topological Hall effect in the A phase of MnSi. *Phys Rev Lett*. 102(18):186602.
28 Lee M, Kang W, Onose Y, Tokura Y, Ong NP. 2009. Unusual Hall effect anomaly in MnSi under pressure. *Phys Rev Lett*. 102(18):186601.
29 Ritz R, *et al.* 2013. Giant generic topological Hall resistivity of MnSi under pressure. *Phys Rev B*. 87(13):134424.
30 Franz C, *et al.* 2014. Real-space and reciprocal-space Berry phases in the Hall effect of $Mn_{1-x}Fe_xSi$. *Phys Rev Lett*. 112(18):186601.
31 Verma N, Addison Z, Randeria M. 2022. Unified theory of the anomalous and topological Hall effects with phase-space Berry curvatures. *Sci Adv*. 8(45):abq2765.
32 Addison Z, Keyes L, Randeria M. 2025. Anomalous and topological Hall effects with phase-space Berry curvatures: electric, thermal, and thermoelectric transport in magnets. *Phys Rev B*. 112(1): 014446.
33 Inosov DS, *et al.* 2009. Electronic structure and nesting-driven enhancement of the RKKY interaction at the magnetic ordering propagation vector in Gd_2PdSi_3 and Tb_2PdSi_3. *Phys Rev Lett*. 102(4):046401.
34 Dong Y, *et al.* 2024. Fermi surface nesting driving the RKKY interaction in the centrosymmetric skyrmion magnet Gd_2PdSi_3. *Phys Rev Lett*. 133(1):016401.
35 Ashcroft NW, Mermin ND. *Solid state physics*. Saunders College Publishing, 1976.
36 Li X, *et al.* 2023. The phonon thermal Hall angle in black phosphorus. *Nat Commun*. 14(1):1027.
37 Uehara T, Ohtsuki T, Udagawa M, Nakatsuji S, Machida Y. 2022. Phonon thermal Hall effect in a metallic spin ice. *Nat Commun*. 13(1):4604.
38 Wang Z, Barros K, Chern G, Maslov DL, Batista CD. 2016. Resistivity minimum in highly frustrated itinerant magnets. *Phys Rev Lett*. 117(20):206601.
39 Simons DS, Salamon MB. 1974. Specific heat and resistivity of gadolinium near the Curie point in external magnetic fields. *Phys Rev B*. 10(11):4680.
40 Fisher ME, Langer JS. 1968. Resistive anomalies at magnetic critical points. *Phys Rev Lett*. 20(13):665.